4448–4457 *Nucleic Acids Research, 2010, Vol. 38, No. 13* *Published online 28 March 2010*
doi:10.1093/nar/gkq173

Visualizing helicases unwinding DNA at the single molecule level

Natali Fili[1], Gregory I. Mashanov[1], Christopher P. Toseland[1], Christopher Batters[1], Mark I. Wallace[1], Joseph T. P. Yeeles[2], Mark S. Dillingham[2], Martin R. Webb[1] and Justin E. Molloy[1,*]

[1]MRC National Institute for Medical Research, Mill Hill, London NW7 1AA and [2]DNA-Protein Interactions Unit, Department of Biochemistry, School of Medical Sciences, University of Bristol, University Walk, Bristol, BS8 1TD, UK

Received January 11, 2010; Revised February 26, 2010; Accepted March 2, 2010

ABSTRACT

DNA helicases are motor proteins that catalyze the unwinding of double-stranded DNA into single-stranded DNA using the free energy from ATP hydrolysis. Single molecule approaches enable us to address detailed mechanistic questions about how such enzymes move processively along DNA. Here, an optical method has been developed to follow the unwinding of multiple DNA molecules simultaneously in real time. This was achieved by measuring the accumulation of fluorescent single-stranded DNA-binding protein on the single-stranded DNA product of the helicase, using total internal reflection fluorescence microscopy. By immobilizing either the DNA or helicase, localized increase in fluorescence provides information about the rate of unwinding and the processivity of individual enzymes. In addition, it reveals details of the unwinding process, such as pauses and bursts of activity. The generic and versatile nature of the assay makes it applicable to a variety of DNA helicases and DNA templates. The method is an important addition to the single-molecule toolbox available for studying DNA processing enzymes.

INTRODUCTION

DNA helicases are ubiquitous motor proteins that are involved in nearly all aspects of DNA metabolism, including replication, recombination and repair. In addition to double-stranded DNA (dsDNA) unwinding, helicases are known to exhibit diverse activities, such as strand degradation (1,2). Recently, single-molecule studies have contributed substantially to the understanding of these multi-functional enzymes. Both mechanical methods, such as optical tweezers (3–5), magnetic tweezers (6–8) and tethered-particle analysis (9,10), and imaging techniques, such as single-pair Förster resonance energy transfer (FRET) (11–13) and microfluidics analysis of fluorescently labeled DNA (14,15) or labeled enzyme (16), have been used to resolve individual enzymes moving along DNA or RNA. These methods have unraveled various key aspects of helicase activity such as processivity, unwinding and translocation mechanisms (4,5,9,12,17), regulation by DNA sequences (9,15,16) as well as protein and DNA conformational changes (11,13,18).

These strategies are very different and hence mutually complementary. For instance, methods that apply external forces, such as optical and magnetic tweezers, allow the activity of an individual helicase molecule to be followed with high temporal and spatial resolution. Lower resolution techniques such as tethered-particle or microfluidic assays can be applied on long DNA substrates and are therefore suitable for processive enzymes. Finally, single-pair FRET, although limited to short DNA substrates, provides the resolution required for measuring intramolecular conformational changes during unwinding.

Here, a method has been developed to follow the unwinding of multiple dsDNA molecules in real time, particularly suited to processive helicases. The method uses the binding of a fluorescently labeled single-stranded DNA-binding protein (SSB) from *Escherichia coli* to single-stranded DNA (ssDNA), in order to produce an optical read-out of helicase activity, by means of total internal reflection fluorescence microscopy (TIRFM). Two experimental approaches were devised, in which

*To whom correspondence should be addressed. Tel: +44 208 816 2591; Fax: +44 20 8906 4477; Email: jmolloy@nimr.mrc.ac.uk
Present address:
Mark I. Wallace, Department of Chemistry, University of Oxford, Chemistry Research Laboratory, Mansfield Road, OX1 3TA, Oxford, UK.

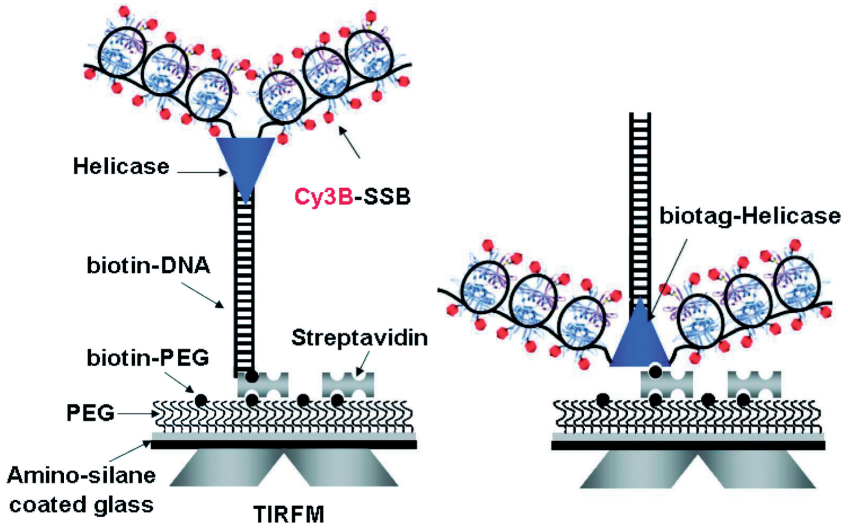

Figure 1. Principle of the helicase assay. Biotinylated dsDNA (**A**) or biotinylated helicase (**B**) is immobilized on the PEGylated surface through biotin–streptavidin interaction. In the presence of ATP, the helicase unwinds its substrate. Fluorescent Cy3B-SSB then specifically binds to the ssDNA product of the helicase. The recruitment of Cy3B-SSB on ssDNA is observed as a localized increase in fluorescence, which reflects the activity of the helicase. To enhance the signal-to-noise ratio, unwinding is visualized by TIRFM.

either biotinylated dsDNA (Figure 1A) or biotinylated helicase (Figure 1B) is immobilized on an inert polyethylene-glycol-coated (PEGylated) surface through biotin–streptavidin interactions. Helicase activity leads to the accumulation of fluorescent SSB molecules on the growing ssDNA products, which results in a localized increase in fluorescence, proportional to the length of ssDNA. This reports the progress of unwinding for individual dsDNA molecules, providing information on the processivity and unwinding rate of the helicase.

SSB is a homotetrameric protein, which specifically binds ssDNA (19,20). At high salt concentrations and low protein-to-DNA ratio, SSB binds with a stoichiometry of ~65 bases per SSB tetramer, whereas at low salt concentration and high protein-to-DNA ratio, binding is favored with a stoichiometry of ~35 bases per tetramer (19). A coumarin-labeled SSB, termed DCC-SSB (21), has been used previously as a fluorescent biosensor suitable for bulk studies. DCC-SSB binds ssDNA tightly (K_d = 2.5 nM) with a 6-fold fluorescence enhancement. Binding is rapid (rate constant 350 $\mu M^{-1} s^{-1}$) and has a stoichiometry similar to the wild-type SSB (22). A variant of this biosensor was optimized for the single-molecule, TIRF-based, measurements reported here.

MATERIALS AND METHODS

TIRF imaging

Single-molecule imaging was performed using a custom-built, objective-coupled TIRFM apparatus, as previously described (23). TIRF excitation was provided by a 532 nm, 50 mW, solid-state laser (Suwtech 532-50 with 1500 LDC controller, SP3-Plus) and the emitted fluorescence was imaged onto an electron-multiplying charge-coupled device (EMCCD, iXon897BV, Andor). A full description of the instrumentation is given in the Supplementary Data. Video data were stored directly on computer hard drive using a frame-grabber card and custom software (see Data analysis section).

Surface preparation

Use of a polyethylene-glycol-(PEG)-coated surface minimized non-specific adsorption of the assay components. Surface chemistry was performed by adapting a protocol previously described (11) and described in detail in the Supplementary Data.

ssDNA biosensors and helicases

Cy3B-maleimide was from GE Healthcare. Cy3B-SSB-W88C and DCC-SSB-G26C were prepared and characterized, essentially as previously described (21). *Bacillus subtilis* $AddA^{D1172A}B^{D961A}$ ($AddA^{N}B^{N}$) and $AddA^{K36A}B$ mutants (21,24), *E. coli* RecBCD (24,25), *B. stearothermophilus* PcrA and *Staphylococcus aureus* RepD (26–28) were purified as described previously. The generation of biotag-$AddA^{N}B^{N}$ is described in detail in the Supplementary Data (24,29–31).

DNA substrates

All oligonucleotides were purchased from Eurogentec Ltd. The DNA substrates for $AddA^{N}B^{N}$ and RecBCD were generated by PCR on the pSP73-JY0 plasmid, which contains a 5.27 kb sequence devoid of Chi_{Bs} and Chi_{Ec} sequences (termed Chi_0 fragments, see Supplementary Data). Using a single 5′-biotin-TEG forward primer and various non-biotinylated reverse primers, pSP73-JY0 was used as template to generate 5′-biotinylated Chi_0 fragments of different lengths. Non-biotinylated fragments were generated for negative control experiments and for studying the activity of immobilized biotag-$AddA^{N}B^{N}$. PcrA substrates were generated using the pCER*Ori*D plasmid (32) as a template. All PCR products were

purified by gel extraction and analyzed by electrophoresis on 1% (w/v) agarose gel.

Single-molecule helicase assays

To study DNA unwinding using surface-immobilized dsDNA, the PEGylated surface of the flow-cell was treated for 15 min with 20 μg/ml streptavidin in 'TB' buffer (TB = 25 mM Tris–HCl, pH 7.5 and 10 mM NaCl) and then incubated for 15 min with biotinylated dsDNA (200–500 pM) in TB buffer. After each step, excess unbound protein or DNA was washed out with TB buffer. Serial dilutions were performed to obtain the optimum surface density of dsDNA templates so the unwinding events appeared as discrete fluorescent spots. For surface-immobilized $AddA^NB^N$, the streptavidin-coated surface was first treated with 2.5 nM biotag-$AddA^NB^N$ in TB buffer and excess protein was washed out as above. Buffer conditions and Cy3B-SSB concentration were chosen to ensure that binding occurs rapidly and at the stoichiometry of 65 bases per SSB tetramer (Supplementary Figures S1 and S7).

To study the activity of the different helicases, the assay was performed as follows: (i) $AddA^NB^N$: the immobilized Chi_0 dsDNA was incubated with 10 nM $AddA^NB^N$ in 'TA' buffer, supplemented with 3 μM or 1 mM ATP [TA = 25 mM Tris–HCl (pH 7.5), 200 mM NaCl, 2 mM $MgCl_2$ and 25 nM Cy3B-SSB]. The activity of immobilized $AddA^NB^N$ was initiated by addition of 1 mM ATP in the presence of 1 nM non-biotinylated dsDNA in TA buffer; (ii) PcrA/RepD: immobilized dsDNA with the *ori*D sequence at its free end was incubated with 500 nM RepD in 'TP' buffer for 30 min [TP = 50 mM Tris–HCl (pH 7.5), 100 mM KCl, 10 mM $MgCl_2$ and 1 mM EDTA] to yield the RepD–DNA complex. PcrA (100 nM) was then added and unwinding initiated with 1 mM ATP in TP buffer supplemented with 25 nM Cy3B-SSB. (iii) RecBCD: immobilized Chi_0 dsDNA was incubated with 10 nM RecBCD in 'TR' buffer supplemented with 2 mM ATP [TR = 25 mM Tris–acetate (pH 7.5), 1 mM CH_3COOMg and 25 nM Cy3B-SSB].

For the calibration of the assay, Cy3B-SSB–DNA complexes of various lengths were generated by incubating 70 pM biotinylated dsDNA for 5 min with 10 nM $AddA^NB^N$ and 1 mM ATP in TA Buffer. The Cy3B-SSB-decorated products of helicase activity were immobilized on the streptavidin-coated PEGylated surface and washed once with 25 nM Cy3B-SSB. Their intensity recorded using identical acquisition parameters to the ones used when helicase assay was performed on the surface.

All experiments were performed at 24°C, in the presence of an oxygen scavenger system (33), consisting of 10 mg/ml glucose, 50 μg/ml glucose oxidase, 400 μg/ml catalase, 500 μg/ml BSA, 1 mM DTT, 1 mM ascorbic acid, 1 mM methyl viologen. Using a laser power of 0.5 mW, the photobleaching rate was $0.009\ s^{-1}$. An ATP regeneration system, consisting of 100 μg/ml creatine phosphokinase and 500 μg/ml creatine phosphate, were also added to the appropriate buffer.

Data analysis

Image analysis was performed using custom-written computer software (freely available at http://www.nimr.mrc.ac.uk/gmimpro/) (34). Individual fluorescent spots were identified by a pattern matching algorithm and the putative target spots were then screened to eliminate those with constant or instantaneously increasing fluorescence. The remaining spots were then analyzed to yield intensity as a function of time. The dataset was analyzed by measuring the duration of unwinding (Δt_{tot}) and total increase in intensity (ΔI_{tot}). To translate the rates from ccp/s to bp/s, we assumed that the mean ΔI_{tot} corresponds to the complete unwinding of 1500 bp, given the known high processivity of AddAB.

To identify and characterize the pauses and unwinding phases a custom-written PERL algorithm (ActiveState Software Inc.) was developed. Each intensity trace was first smoothed by running average and then used to calculate the first derivative trace as a function of time. Thresholding (*Thr.*) of the first derivative trace was used to segment the trace into the two phases: the unwinding phases were identified as the regions for which the derivative was $>Thr$. To automate the analysis, one set of criteria was applied for all traces. Given the high variability in the shape and the noise of the intensity traces, a window size of 21 points was chosen after optimization for the running average smoothing. The general principle of the algorithm is described in Figure 5A and Supplementary Data. Artificial data sets were generated to estimate the contribution of experimental noise and verify the threshold level used to identify pauses and bursts in the original data sets (see Results section and Supplementary Figure S8).

Stopped-flow measurements

Stopped-flow experiments were carried out using a HiTech SHU-61SX2 (TgK scientific Ltd.) with a mercury–xenon light source (excitation: 436 nm; emission: 455 nm cut-off filter (Schott glass) and HiTech IS-2 software. DNA unwinding was monitored using the DCC-SSB which provides a ~6-fold increase in fluorescence upon DNA binding (21). Experiments were performed at 24°C, in the same buffers used for single-molecule assays. However, 25 nM DCC-SSB tetramers were substituted for the Cy3B-SSB. To simulate the surface immobilization, 150 pM biotinylated DNA was pre-incubated for 5 min with 1.5 nM streptavidin and then with 5 nM $AddA^NB^N$. Helicase unwinding was initiated by rapid mixing with an equal volume of 1 mM ATP in the same buffer. The quoted concentrations are those in the mixing chamber.

RESULTS

Development of the DNA unwinding assay

The assay was based on TIRFM, which in combination with a sensitive, electron-multiplying, CCD camera, provides high temporal resolution and high signal-to-noise ratio. A Cy3B-labeled W88C mutant of SSB, termed

Cy3B-SSB, was used to probe the ssDNA product of the helicase. Labeling was performed as previously described (21), so that each SSB monomer contains one Cy3B. Cy3B was selected for its high photostability, high quantum yield and long excitation and emission wavelengths. Bulk analysis showed that Cy3B-SSB binds ssDNA tightly ($K_d < 2.5$ nM), with 1.8-fold fluorescence increase upon binding (data not shown). The high affinity of Cy3B-SSB for ssDNA was confirmed by TIRFM, using surface-immobilized, biotinylated dT_{80}, which should bind only one tetramer at high salt concentration (Supplementary Figure S1). Indeed, each Cy3B-SSB–ssDNA complex appeared as a diffraction-limited fluorescent spot, which at high laser power exhibited four-step photobleaching, as expected for the 1:1 tetramer–dT_{80} complex. This four-step photobleaching supports the idea that the SSB is binding in the 65-base mode for these conditions. Each stepwise decrease in intensity was of similar magnitude to the fluorescence intensity of a single Cy3B fluorophore. Spot lifetime was dependent upon both photobleaching, which is proportional to laser power, and complex dissociation, which is independent of laser power. Measurement of the spot's lifetime at different laser powers gave an estimated dissociation rate constant of $<0.005\,s^{-1}$ (Supplementary Figure S2), consistent with Cy3B-SSB binding tightly to ssDNA.

The conditions of the unwinding assay were selected to ensure rapid binding to ssDNA at the stoichiometry of 65 bases per SSB tetramer. Experiments were performed at 25 nM Cy3B-SSB, which is 10-fold higher than its K_d value measured under similar conditions (22). Furthermore, at 25 nM SSB tetramers, the binding rate to ssDNA will be $36 \times 10^8\,M^{-1}\,s^{-1} \times 25\,nM = 9$ SSB per second, equivalent to ~600 bp/s unwinding rate (22). So, this ensures that 65-base binding should predominate, the observed rate of DNA unwinding is not limited by the rate of SSB binding (Supplementary Figure S7) and that background fluorescence from free Cy3B-SSB in the bulk solution is minimized (Supplementary Figure S8). Finally, oxygen scavenger conditions were specifically optimized to minimize Cy3B photobleaching to a rate of $0.009\,s^{-1}$.

Finally, to establish the relationship between fluorescence intensity and DNA length, the final products of helicase activity were generated in solution in the presence of Cy3B-SSB, using different lengths of biotinylated dsDNA fragments as substrates. The Cy3B-SSB-decorated products of unwinding were surface-immobilized and their fluorescence was measured by TIRFM (Supplementary Figure S3). Mean intensity was proportional to DNA fragment length up to 2 kb. However, beyond this, the relationship became non-linear probably because larger complexes were not fully illuminated by the evanescent wave, which decays exponentially with distance from the surface.

Visualizing the helicase activity of $AddA^NB^N$

The assay was first exemplified using the activity of *B. subtilis* AddAB, which is a helicase-nuclease with an essential role in the initiation of DNA recombination (35,36). AddAB contains a single helicase motor domain in the A subunit and two nuclease domains at the C-terminus of A and B subunits (35). It binds to blunt ends of dsDNA with high affinity and unwinds the duplex in an ATP-dependent manner, while simultaneously degrading the ssDNA product (24,37). AddAB is a highly processive helicase with activity regulated by a specific DNA sequence (5′-AGCGG-3′) termed Chi_{Bs} (36). In order to avoid effects due to Chi and to strand degradation, the nuclease-inactive mutant $AddA^{D1172A}B^{D961A}$ ($AddA^NB^N$) (24) was used on a dsDNA substrate, devoid of Chi_{Bs} (Chi_0). Biotinylated 1.5 kb dsDNA was immobilized on the surface and incubated with $AddA^NB^N$. Helicase activity was initiated by addition of ATP in the presence of Cy3B-SSB and surface fluorescence was observed by TIRFM (Figure 2A). A series of control experiments showed that the appearance of fluorescence spots was specifically due to $AddA^NB^N$ helicase activity (Supplementary Figure S4A).

The time-course of the unwinding reaction was monitored by following the accumulation of Cy3B-SSB on the ssDNA product. The fluorescence intensity gradually increased (Figure 2B, Supplementary Figure S4B, and Movie 1) to a maximum value before a single- (Figure 2B) or a two-step (Supplementary Figure S4C) decrease to background level. This decrease probably corresponds to the simultaneous or sequential release of the two ssDNA products. The release of the biotinylated ssDNA is consistent with $AddA^NB^N$ being able to disrupt the biotin–streptavidin interaction, as described for wild-type AddAB (31) and other helicases (38,39). Interestingly, the intensity trace indicates that unwinding does not occur at a constant rate, but rather involves pauses and bursts of activity, which will be explored further below.

The intensity time-course for each unwinding event was characterized by two parameters: total increase in intensity (ΔI_{tot}) and total duration of unwinding (Δt_{tot}) (Figure 2B). The distribution of these parameters provides information about the helicase processivity and the heterogeneity of its activity and will be explored further later. Moreover, assuming complete unwinding of the 1.5 kb substrate, Δt_{tot} provides an estimate of the apparent unwinding rate U_r in base pairs per second (bp/s) ($U_r = 1500/\Delta t_{tot}$). For $AddA^NB^N$, U_r had an average value of 82 bp/s (SD, 63 bp/s) (Supplementary Figure S5A).

Visualizing DNA unwinding by different helicases

To explore its generic nature, the assay was also used to monitor the activity of two well-studied bacterial helicases in their wild-type form. PcrA is a helicase from *B. stearothermophilus* involved in plasmid replication (40,41), and RecBCD, a trimeric helicase-nuclease from *E. coli*, which is involved in the recombinatorial repair of DNA breaks (1). The exact details of the unwinding by these two helicases was not fully explored in this study, rather they were used to exemplify the fact that this assay could be extended to different processive

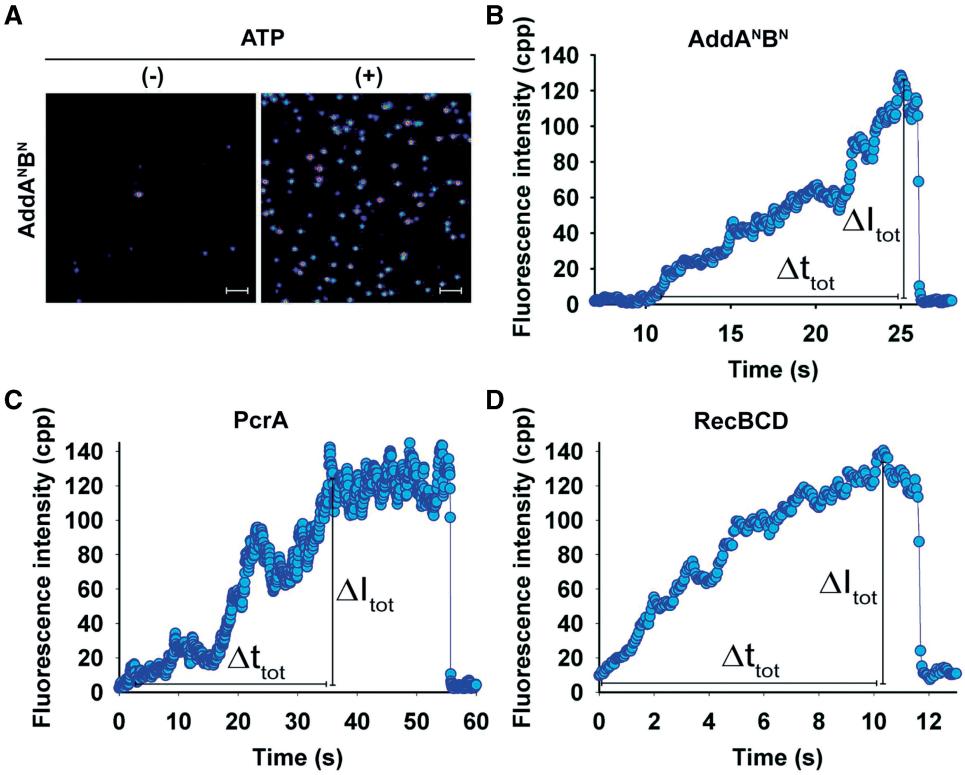

Figure 2. Monitoring unwinding of single DNA molecules by three helicases. (**A** and **B**) Biotinylated Chi_0 dsDNA (1.5 kb) was immobilized on the PEGylated surface and incubated with the nuclease-inactive mutant, $AddA^NB^N$, in the presence of Cy3B-SSB. Helicase activity was initiated with 1 mM ATP and video images of the surface fluorescence signal were acquired at 20 Hz using TIRFM. Discrete fluorescent spots of increasing intensity appeared as individual DNA molecules were being progressively unwound. (B) Representative intensity time-course for $AddA^NB^N$ showing the simultaneous release of the two ssDNA strands. (**C**) Immobilized 1.5 kb dsDNA containing the *ori*D sequence at its free-end was first incubated with RepD and then with PcrA and Cy3B-SSB. Helicase activity was initiated with 1 mM ATP. Representative trace of a PcrA unwinding event is shown. (**D**) Immobilized 1.5-kb Chi_0 dsDNA was incubated with 1 mM ATP and Cy3B-SSB, under conditions of low Mg^{2+} concentration which suppresses its nuclease activity. Helicase activity was initiated by addition of RecBCD. Representative trace of a RecBCD unwinding event is shown. The two parameters used to define unwinding: the total event duration (Δt_{tot}) and the total increase in intensity (ΔI_{tot}), are shown here.

helicases. The conditions, such as SSB concentration, were not optimized for each helicase.

PcrA activity was monitored using an immobilized 1.5 kb substrate containing the double-stranded origin of replication sequence *ori*D (28) at its free-end. Replication initiator protein, RepD, binds and nicks the DNA at this sequence allowing PcrA to load and actively unwind. Following nicking of *ori*D by RepD (28,42) and addition of ATP, single unwinding events were observed as for $AddA^NB^N$ (Figure 2C, Supplementary Figure S6A). The average Δt_{tot} for PcrA was 48 s (SD, 20 s) and the average apparent unwinding rate was estimated to be 38 bp/s (SD, 24 bp/s), similar to the 30 bp/s reported using bulk methods (27).

To monitor DNA unwinding by RecBCD, the experiment was performed under low free Mg^{2+} conditions which suppress its nuclease activity (1) (Supplementary Figure S6B). For simplicity, the DNA was devoid of the octameric sequence $Chi_{E.c}$ that regulates RecBCD activity (14–16). A representative intensity time-course of RecBCD activity on immobilized 1.5 kb DNA is shown in Figure 2D. The average Δt_{tot} for RecBCD was 15 s (SD, 15 s) and the average apparent unwinding rate was estimated to be 200 bp/s (SD, 175 bp/s) similar the value (250 bp/s) measured at 25°C in bulk solution studies (43). However, as outlined above, the rate of SSB binding may contribute to rate limitation for RecBCD.

As exemplified by the intensity traces (Figure 2B–D), RecBCD exhibits a higher overall unwinding rate than $AddA^NB^N$ and PcrA, consistent with previous observations (21,27). Moreover, similar to $AddA^NB^N$, unwinding by both enzymes is characterized by pauses and bursts of activity. Although an extensive analysis of these two helicases was beyond the scope of this study, these two examples clearly demonstrate that this approach is widely applicable to other DNA helicases and is able to detect differences in their activity.

DNA unwinding by immobilized helicase

In principle, with immobilize DNA and helicase in solution, it is possible that the helicase dissociates prior to complete unwinding and is replaced by a fresh helicase molecule. In practice with AddAB this is unlikely as it only binds to blunt ends (36). To test whether a single helicase molecule is responsible for the observed unwinding activity, an alternative immobilization strategy was used (Figure 1B). Biotag-$AddA^NB^N$ was coupled to the PEGylated surface and a non-biotinylated version of the

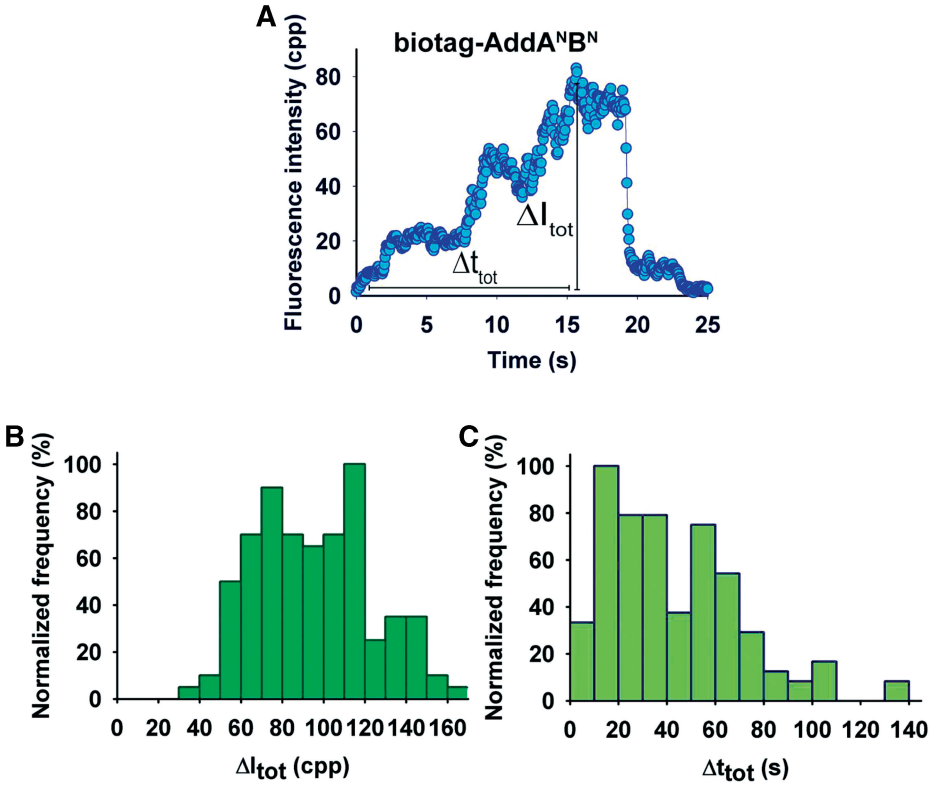

Figure 3. DNA unwinding by immobilized AddA^{N}B^N. Biotag-AddA^{N}B^N was immobilized on PEGylated surfaces and incubated with 1 mM ATP in the presence of Cy3B-SSB. Multiple unwinding events were initiated by addition of 1.5 kb non-biotinylated Chi_0 dsDNA and observed as fluorescent spots of increasing intensity. (**A**) Intensity trace of a representative unwinding event. The time course of 128 events was analyzed as described in the text. The distribution of ΔI_{tot} (**B**) and Δt_{tot} (**C**) is presented as percentage frequency, normalized to the maximum.

same 1.5 kb Chi_0 DNA fragment was used. Fluorescence changes were then measured as before (Supplementary Figure S6C). Similar to the activity of AddA^{N}B^N on immobilized DNA, the time-course of unwinding at 1 mM ATP was characterized by pauses and bursts of activity (Figure 3A). This similarity (compare with Figure 2B) demonstrates that the pausing phenomenon was not an experimental artifact of the DNA immobilization. In addition, the distributions of ΔI_{tot} and Δt_{tot} were broad with a mean of 95 counts per pixel (cpp) (SD, 28 cpp) and 43 s (SD, 28 s), respectively (Figure 3B and C) and the average apparent unwinding rate was estimated to be 60 bp/s (SD, 67 bp/s). The slightly lower rate of unwinding observed for immobilized AddA^{N}B^N could be attributed to the effect of immobilization on its activity. However, the overall similarity between the two experimental approaches (compare with Figure 4A and B) suggests that the pauses and bursts of activity we observe describe the activity of a single helicase molecule moving along a single DNA template.

AddA^{N}B^N unwinding rate is ATP dependent

The helicase activity of AddA^{N}B^N on immobilized DNA was investigated in more detail. The distributions of ΔI_{tot} and Δt_{tot} at saturating ATP concentration are shown in Figure 4A and B, respectively. Both distributions were broad, indicative of heterogeneity within the AddA^{N}B^N population, which has been previously reported for other helicases (14,16). ΔI_{tot} had a mean of 92 cpp (SD, 29 cpp), in agreement with the calibration data (Supplementary Figure S3C), and Δt_{tot} an average of 31 s (SD, 25 s). The rate of unwinding was not limited by Cy3B-SSB binding, since doubling its concentration did not significantly change the average Δt_{tot} (Supplementary Figure S7). To test whether the duration and extent of completion of unwinding were ATP dependent experiments were performed at sub-saturating (3 μM) ATP concentrations and results compared to saturating conditions (1 mM ATP). As demonstrated by Figure 4A, ΔI_{tot} was ATP independent with mean of 96 cpp (SD, 30 cpp) at 3 μM ATP, consistent with complete unwinding of the 1.5 kb substrate. Unlike ΔI_{tot}, the distribution of Δt_{tot} was strongly dependent on ATP concentration (Figure 4B). At 3 μM ATP, the average Δt_{tot} increased to 171 s (SD, 138 s) and therefore the estimated mean U_r decreased to13 bp/s (SD, 7 bp/s).

Ensemble averaging enables comparison to bulk measurements

The unwinding activity of AddA^{N}B^N was also measured in bulk solution using rapid-mixing, stopped-flow, methodology. The DCC-SSB probe (21) was used to monitor unwinding. The fluorescence trace shows an initial lag, followed by an approximately linear increase and then a phase of gradually decreasing rate, to a maximum value (Figure 4C). The rate of the linear phase of the unwinding reaction was 65 bp/s, similar to the 82 bp/s calculated from the Δt_{tot} distribution (Supplementary Figure S5A). In

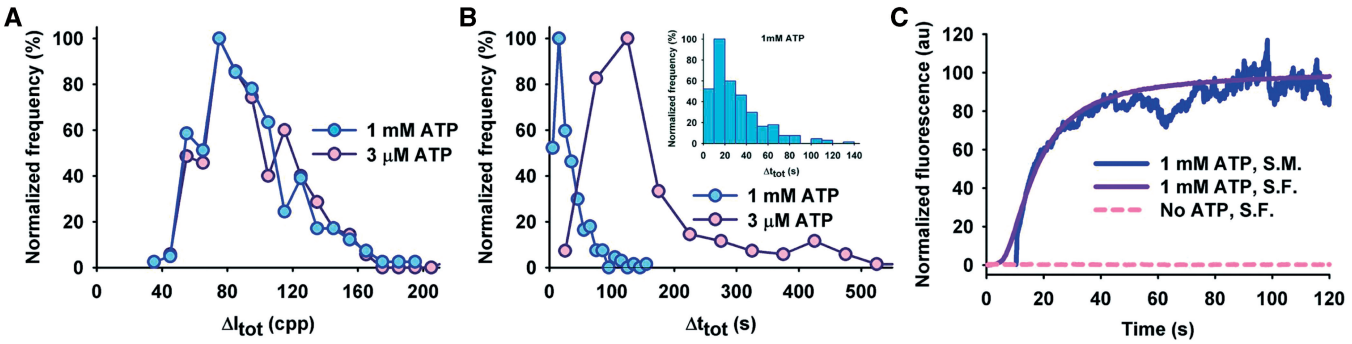

Figure 4. DNA unwinding by AddA^{N}B^{N} in bulk and at single molecule level. (**A** and **B**) The activity of AddA^{N}B^{N} on immobilized 1.5 kb Chi_0 dsDNA was observed as in Figure 2 at 1 mM and 3 μM ATP. Images were acquired at 20 and 5 Hz, respectively, and individual unwinding events from three independent experiments (1mM ATP, $n = 233$; 3 μM ATP, $n = 200$) were analyzed, as described in the text. The distributions of ΔI_{tot} (A) and Δt_{tot} (B) are presented as percentage frequency, normalized to the maximum. The inset in (B) shows the distribution of Δt_{tot} for 1 mM ATP. (**C**) A representative stopped-flow (S.F.) trace reporting the ensemble activity of AddA^{N}B^{N} on the same 1.5 kb biotinylated DNA fragment at 1 mM ATP. For direct comparison with the single-molecule data (S.M.), the substrate was pre-incubated with excess of streptavidin to ensure unidirectional unwinding. The stopped-flow trace is overlaid with the ensemble-averaged trace of 233 individual unwinding events that were synchronized to their start point and averaged. The S.M. trace has been shifted in the time axis to synchronize the onset of fluorescence increase. Both traces were normalized to the maximum.

addition, the gradual reduction in rate towards the end of the reaction is in agreement with the broad dispersion of Δt_{tot} values found in the single-molecule data. The overall similarity between the two experimental approaches is demonstrated when the ensemble-averaged trace of the single-molecule data is compared to the stopped-flow measurements (Figure 4C). The stopped-flow trace shows a lag phase before unwinding commences and this lag cannot be identified in the single-molecule records, because the 'zero time' is not defined as in stopped-flow measurements. However, the phase of fluorescence increase can be synchronized and is found to occur with very similar kinetics for both types of experiment.

AddA^{N}B^{N} helicase exhibits pauses and bursts of activity

To further explore the activity of AddA^{N}B^{N}, the intensity time-courses of multiple unwinding events were closely examined. Assuming that the Δt_{tot} for each completed unwinding event is the result of n individual steps along the 1.5 kb DNA molecule (each step being an independent Poisson process), the distribution of Δt_{tot} for individual molecules is expected to be narrow, with a mean of n/U_r and a standard deviation of $n^{0.5}/U_r$. Assuming that AddA^{N}B^{N} moves in single base steps, as seen for example with the closely related helicase PcrA (27), n would be = 1500 and therefore, the distribution of Δt_{tot} would have a mean of 31 s with a SD of 0.5 s. However, the observed distribution of Δt_{tot} was much broader, suggesting a kinetic heterogeneity, which has also been reported for other helicases (5,14). The heterogeneity cannot be attributed to premature termination of unwinding, since there is no correlation between the individual values of Δt_{tot} and ΔI_{tot} (Supplementary Figure S5B). Hence, we propose that the broad distribution arises because the unwinding process consists of pauses and bursts of activity, as shown in Figure 2B.

Examination of individual intensity time-courses (Figures 2B and 5A, and Supplementary Figure S4C) reveals that unwinding occurs in two different phases: rapid increases in fluorescence (bursts or unwinding phases) interrupted by periods of constant or even decreasing intensity (pauses). To analyze the two phases, the first derivative of each time-course was calculated (Figure 5A). By thresholding the first derivative data the two phases could be discriminated so that the number and duration of the pauses and the maximum rate and duration of the bursts could be estimated. To test whether these phases were due to random intensity fluctuations, due to movement of the Cy3-SSB decorated DNA product, the experimental data were compared to artificial datasets in which time-courses of increasing intensity were simulated. To this end, the intensity fluctuations of Cy3B-SSB-decorated fully unwound DNA substrates of various lengths were recorded over time under identical conditions (Supplementary Figure S8A). Using the known relationship between noise and intensity (Supplementary Figure S8B), and assuming a linear increase in intensity over time, these fluctuations were converted into artificial time-courses which could be directly compared to the original experimental data (Supplementary Figure S8C). The distribution of the first derivative of the simulated data was used to set the optimum threshold to detect pauses and bursts of activity and estimate the incidence of false and missing events (Supplementary Figure S8D). This threshold was set at 10 cpp/s for 1 mM ATP and 1.5 cpp/s for 3 μM ATP.

At 1 mM ATP, AddA^{N}B^{N} exhibited on average three pauses (SD, one pause) with a mean duration of 4 s (SD, 4 s) (Figure 5B and C). Therefore, during the unwinding of the 1.5 kb substrate, AddA^{N}B^{N} spends, on average, 40% of the time in the paused state. The number of pauses was not significantly dependent on ATP concentration, since, at 3 μM ATP, the enzyme also stalled on average three times (SD, two pauses) (Figure 5B). The pause duration increased to 21 s (SD, 21 s) at 3 μM ATP (Figure 5C), indicating that exit from the paused state requires ATP binding.

The bursts of unwinding were strongly dependent on the concentration of ATP. At 1 mM ATP, the burst

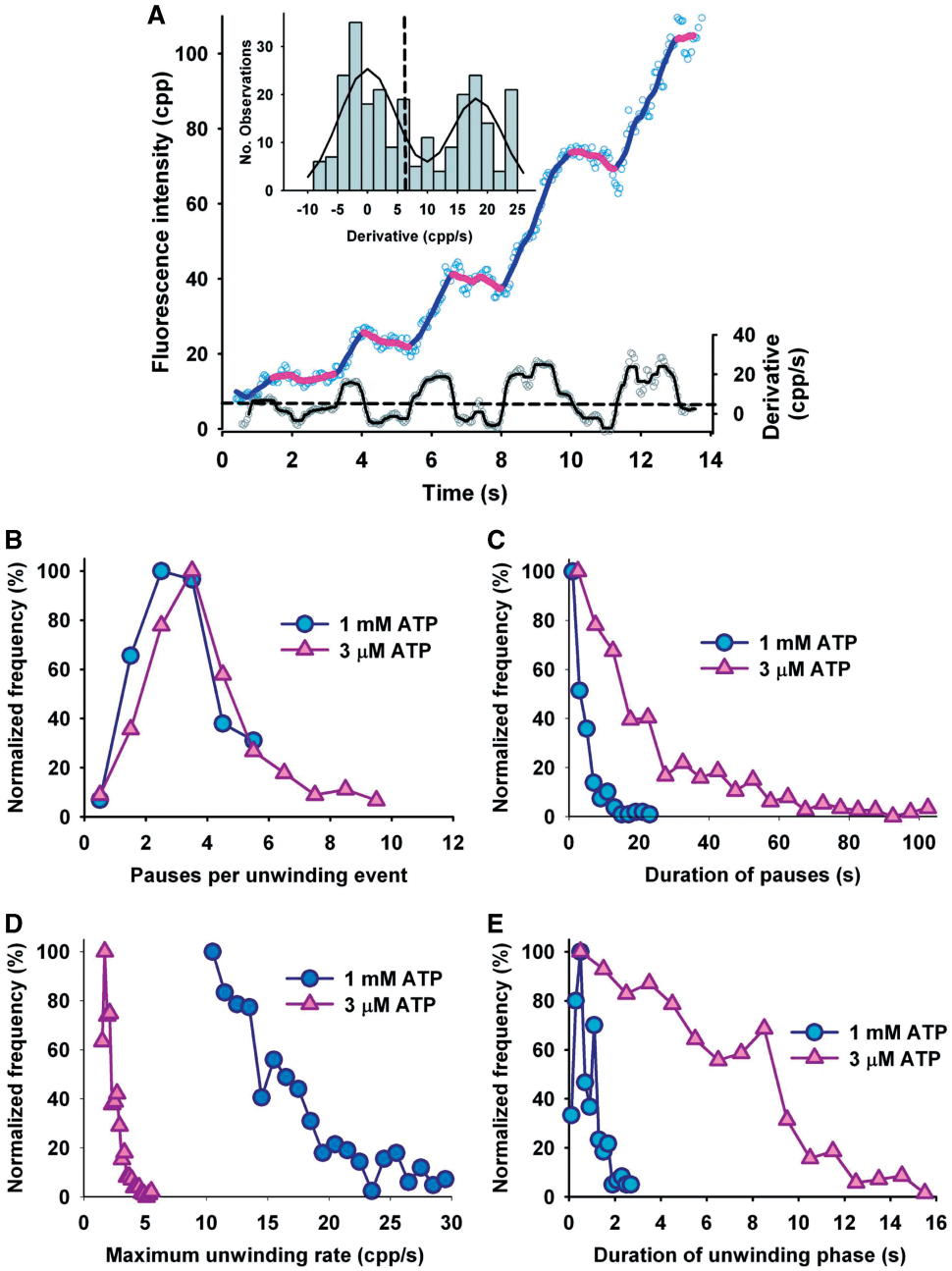

Figure 5. DNA unwinding by $AddA^{N}B^{N}$ is characterized by pauses and bursts of activity. (**A**) Example of how a single time-course can be segmented into pauses and unwinding phases. The raw intensity data (light blue open circle) were smoothed by running average using an optimum window size (shown as pink and dark blue lines). Then, the first derivative at every time point was calculated (grey open circle). If the derivative trace (grey open circle) is smoothed using an median filter (black line), then the histogram of the smoothed derivative values (inset) reveals two populations, one corresponding the pauses (clustered around zero) and one to the unwinding phases (clustered around 17 cpp). Thresholding (*Thr.*) of the derivative data (dashed line) allows the original intensity trace to be segmented into pauses (<*Thr.*, pink lines) and unwinding phases (>*Thr.*, dark lines). (**B–E**) To automatically analyze all data, a custom-written PERL algorithm was used (see 'Materials and methods' section). Using this algorithm, the distributions of the number of pauses per event (B), the duration of pauses (C), maximum rate of unwinding (D) and duration of unwinding phase (E) were obtained for 1 mM ATP (circle) and 3 μM ATP (triangle). All distributions are presented as percentage frequency, normalized to the maximum.

phases had an average maximum rate of 15.6 cpp/s (SD, 4.7 cpp/s) (equivalent to 253 bp/s) and a mean duration of 0.8 s (SD, 0.6 s) (Figure 5D and E). However, at 3 μM ATP, the maximum observed unwinding rate was reduced to a mean value of 2.3 cpp/s (SD, 0.7 cpp/s) (equivalent to 35 bp/s) and the burst duration increased to 4.8 s (SD, 3.4 s) (Figure 5D and E). The difference between the maximum (253 bp/s) and overall average rate of unwinding (U_r = 82 bp/s) (Supplementary Figure S5A) shows that pausing is a dominant phase during unwinding and, if ignored, leads to underestimation of the maximum rate.

DISCUSSION

The method, described here, enables DNA unwinding to be measured in real time by visualizing the recruitment of Cy3B-SSB onto the ssDNA product of the helicase. SSB accumulation results in a localized increase in fluorescence which reports the progress of unwinding. The approach is generally applicable to different DNA helicases and DNA templates under controlled conditions. Surface attachment of either the helicase or its dsDNA substrate via biotin–streptavidin linkage enables the activity of many individual unwinding events to be measured simultaneously by wide-field TIRFM imaging. Moreover, statistical analysis of individual events enables heterogeneity of enzyme activity during an individual event to be studied.

We found that the AddAB unwinding reaction consists of pauses and bursts of activity. Pause duration was strongly ATP dependent, indicating that exit from the paused state requires ATP binding. Such ATP dependence has been previously observed for the helicase NS3 (4). Pausing was observed for all three helicases used in this study and has also been reported for other helicases (4,5,8,12,44). In addition, the high similarity of results, obtained with free and immobilized AddAB, indicate that these pauses and bursts result from just a single helicase enzyme, rather than any dissociation–reassociation of AddAB. One possibility is that pausing might be induced by specific sequences within the DNA substrate. However, ensemble averaging of the individual data records shows that pauses do not occur at the same positions along the 1.5 kb dsDNA substrate. An alternative explanation is that DNA unwinding leads to build-up of torsional forces that cause the enzyme to stall in a stochastic fashion and the enzyme only restarts after a mechanical rearrangement of the DNA. This type of model would be consistent with the finding that the number of pauses is relatively insensitive to ATP concentration.

Pauses were often characterized by a decrease in fluorescence intensity. At present we do not understand the cause of this phenomenon that is presumably occurring while the helicase is stalled and no new ssDNA is being produced. Photobleaching would only account for a decrease of ~4% over a 5 s period. Intensity decreases could be attributed to intensity fluctuations due to noise as well as motion of the immobilized DNA substrate, as indicated by the analysis of the artificial traces. Alternatively, the decrease could be due to the slow rearrangement of SSB along DNA (22,45) resulting in some 35-base binding mode or partial loss of Cy3B-SSB due to tension that is built up in the leading dsDNA. These observations might belie mechanistic details of the helicase and clearly warrant further detailed study.

Other approaches, in which single molecules are manipulated using optical or magnetic tweezers have also revealed pausing and even reversal of helicase movement (4,5,8). The current assay is complementary to these methods since it is performed with no external load and using SSB which is a natural component of the system. When considered together, the results imply that pauses and bursts of activity are important features of helicase activity that are likely to occur under *in vivo* conditions. An advantage of the current assay is that it is based around a bulk assay that uses a very similar biosensor (21). This enables direct comparison between single-molecule and bulk measurements, which is particularly important in order to interpret the single-molecule data. Also, because no extrinsic load is applied to the DNA–helicase complex the measured activity of the enzyme is likely to be close to that found *in vivo*. Further developments, for instance, the use of laminar flow to extend the dsDNA substrates near the surface (14–16), should extend the linear range of dsDNA length beyond the current limit of 2 kb. This might also enable the localization of pauses and bursts of activity along the DNA template by measuring the position of the growing Cy3B-SSB–ssDNA complex. In combination with fluorescently labeled helicases or nucleotides, the assay could also address, at the single-molecule level, questions regarding helicase oligomerization or ATPase kinetics. Finally, given that ssDNA and SSB are both key players in cellular DNA transactions, this new approach could bring the power of single-molecule analysis to the study of many aspects of DNA replication, recombination and repair.

SUPPLEMENTARY DATA

Supplementary Data are available at NAR Online.

ACKNOWLEDGEMENTS

The authors thank K. Tibbles, A. Chavda and C. Morris (NIMR, London) for preparing labeled SSB. They also thank Dr A. Slatter for providing the pCER*Ori*D plasmid.

FUNDING

Grant in Aid from Medical Research Council UK, Wellcome Trust (grant numbers 061523 and 082960) and Royal Society (to M.S.D.); Biotechnology and Biological Sciences Research Council (to J.T.P.Y.). Funding for open access charge: Medical Research Council, UK.

Conflict of interest statement. None declared.

REFERENCES

1. Dillingham,M.S. and Kowalczykowski,S.C. (2008) RecBCD enzyme and the repair of double-stranded DNA breaks. *Microbiol. Mol. Biol. Rev.*, **72**, 642–671.
2. Singleton,M.R., Dillingham,M.S. and Wigley,D.B. (2007) Structure and mechanism of helicases and nucleic acid translocases. *Annu. Rev. Biochem.*, **76**, 23–50.
3. Cheng,W., Dumont,S., Tinoco,I. Jr and Bustamante,C. (2007) NS3 helicase actively separates RNA strands and senses sequence barriers ahead of the opening fork. *Proc. Natl Acad. Sci. USA*, **104**, 13954–13959.
4. Dumont,S., Cheng,W., Serebrov,V., Beran,R.K., Tinoco,I. Jr, Pyle,A.M. and Bustamante,C. (2006) RNA translocation and unwinding mechanism of HCV NS3 helicase and its coordination by ATP. *Nature*, **439**, 105–108.

5. Perkins,T.T., Li,H.W., Dalal,R.V., Gelles,J. and Block,S.M. (2004) Forward and reverse motion of single RecBCD molecules on DNA. *Biophys. J.*, **86**, 1640–1648.
6. Amit,R., Gileadi,O. and Stavans,J. (2004) Direct observation of RuvAB-catalyzed branch migration of single Holliday junctions. *Proc. Natl Acad. Sci. USA*, **101**, 11605–11610.
7. Dawid,A., Croquette,V., Grigoriev,M. and Heslot,F. (2004) Single-molecule study of RuvAB-mediated Holliday-junction migration. *Proc. Natl Acad. Sci. USA*, **101**, 11611–11616.
8. Dessinges,M.N., Lionnet,T., Xi,X.G., Bensimon,D. and Croquette,V. (2004) Single-molecule assay reveals strand switching and enhanced processivity of UvrD. *Proc. Natl Acad. Sci. USA*, **101**, 6439–6444.
9. Dohoney,K.M. and Gelles,J. (2001) Chi-sequence recognition and DNA translocation by single RecBCD helicase/nuclease molecules. *Nature*, **409**, 370–374.
10. Fan,H.F. and Li,H.W. (2009) Studying RecBCD helicase translocation along Chi-DNA using tethered particle motion with a stretching force. *Biophys J.*, **96**, 1875–1883.
11. Ha,T., Rasnik,I., Cheng,W., Babcock,H.P., Gauss,G.H., Lohman,T.M. and Chu,S. (2002) Initiation and re-initiation of DNA unwinding by the Escherichia coli Rep helicase. *Nature*, **419**, 638–641.
12. Myong,S., Bruno,M.M., Pyle,A.M. and Ha,T. (2007) Spring-loaded mechanism of DNA unwinding by hepatitis C virus NS3 helicase. *Science*, **317**, 513–516.
13. Rasnik,I., Myong,S., Cheng,W., Lohman,T.M. and Ha,T. (2004) DNA-binding orientation and domain conformation of the E. coli rep helicase monomer bound to a partial duplex junction: single-molecule studies of fluorescently labeled enzymes. *J. Mol. Biol.*, **336**, 395–408.
14. Bianco,P.R., Brewer,L.R., Corzett,M., Balhorn,R., Yeh,Y., Kowalczykowski,S.C. and Baskin,R.J. (2001) Processive translocation and DNA unwinding by individual RecBCD enzyme molecules. *Nature*, **409**, 374–378.
15. Spies,M., Bianco,P.R., Dillingham,M.S., Handa,N., Baskin,R.J. and Kowalczykowski,S.C. (2003) A molecular throttle: the recombination hotspot chi controls DNA translocation by the RecBCD helicase. *Cell*, **114**, 647–654.
16. Handa,N., Bianco,P.R., Baskin,R.J. and Kowalczykowski,S.C. (2005) Direct visualization of RecBCD movement reveals cotranslocation of the RecD motor after chi recognition. *Mol. Cell*, **17**, 745–750.
17. Spies,M., Amitani,I., Baskin,R.J. and Kowalczykowski,S.C. (2007) RecBCD enzyme switches lead motor subunits in response to chi recognition. *Cell*, **131**, 694–705.
18. Myong,S., Rasnik,I., Joo,C., Lohman,T.M. and Ha,T. (2005) Repetitive shuttling of a motor protein on DNA. *Nature*, **437**, 1321–1325.
19. Lohman,T.M. and Ferrari,M.E. (1994) Escherichia coli single-stranded DNA-binding protein: multiple DNA-binding modes and cooperativities. *Annu. Rev. Biochem.*, **63**, 527–570.
20. Raghunathan,S., Kozlov,A.G., Lohman,T.M. and Waksman,G. (2000) Structure of the DNA binding domain of E. coli SSB bound to ssDNA. *Nat. Struct. Biol.*, **7**, 648–652.
21. Dillingham,M.S., Tibbles,K.L., Hunter,J.L., Bell,J.C., Kowalczykowski,S.C. and Webb,M.R. (2008) Fluorescent single-stranded DNA binding protein as a probe for sensitive, real-time assays of helicase activity. *Biophys. J.*, **95**, 3330–3339.
22. Kunzelmann,S., Morris,C., Chavda,A.P., Eccleston,J.F. and Webb,M.R. (2010) Mechanism of interaction between single-stranded DNA binding protein and DNA. *Biochemistry*, **49**, 843–852.
23. Mashanov,G.I., Tacon,D., Knight,A.E., Peckham,M. and Molloy,J.E. (2003) Visualizing single molecules inside living cells using total internal reflection fluorescence microscopy. *Methods*, **29**, 142–152.
24. Yeeles,J.T. and Dillingham,M.S. (2007) A dual-nuclease mechanism for DNA break processing by AddAB-type helicase-nucleases. *J. Mol. Biol*, **371**, 66–78.
25. Singleton,M.R., Dillingham,M.S., Gaudier,M., Kowalczykowski,S.C. and Wigley,D.B. (2004) Crystal structure of RecBCD enzyme reveals a machine for processing DNA breaks. *Nature*, **432**, 187–193.
26. Bird,L.E., Brannigan,J.A., Subramanya,H.S. and Wigley,D.B. (1998) Characterisation of Bacillus stearothermophilus PcrA helicase: evidence against an active rolling mechanism. *Nucleic Acids Res.*, **26**, 2686–2693.
27. Slatter,A.F., Thomas,C.D. and Webb,M.R. (2009) PcrA helicase tightly couples ATP hydrolysis to unwinding double-stranded DNA, modulated by the initiator protein for plasmid replication, RepD. *Biochemistry*, **48**, 6326–6334.
28. Thomas,C.D., Balson,D.F. and Shaw,W.V. (1990) In vitro studies of the initiation of staphylococcal plasmid replication. Specificity of RepD for its origin (oriD) and characterization of the Rep-ori tyrosyl ester intermediate. *J. Biol. Chem.*, **265**, 5519–5530.
29. Beckett,D., Kovaleva,E. and Schatz,P.J. (1999) A minimal peptide substrate in biotin holoenzyme synthetase-catalyzed biotinylation. *Protein Sci.*, **8**, 921–929.
30. Chedin,F., Handa,N., Dillingham,M.S. and Kowalczykowski,S.C. (2006) The AddAB helicase/nuclease forms a stable complex with its cognate chi sequence during translocation. *J. Biol. Chem.*, **281**, 18610–18617.
31. Yeeles,J.T., Cammack,R. and Dillingham,M.S. (2009) An iron-sulfur cluster is essential for the binding of broken DNA by AddAB-type helicase-nucleases. *J. Biol. Chem.*, **284**, 7746–7755.
32. Zhang,W., Dillingham,M.S., Thomas,C.D., Allen,S., Roberts,C.J. and Soultanas,P. (2007) Directional loading and stimulation of PcrA helicase by the replication initiator protein RepD. *J. Mol. Biol.*, **371**, 336–348.
33. Vogelsang,J., Kasper,R., Steinhauer,C., Person,B., Heilemann,M., Sauer,M. and Tinnefeld,P. (2008) A reducing and oxidizing system minimizes photobleaching and blinking of fluorescent dyes. *Angew. Chem. Int. Ed. Engl.*, **47**, 5465–5469.
34. Mashanov,G.I. and Molloy,J.E. (2007) Automatic detection of single fluorophores in live cells. *Biophys. J.*, **92**, 2199–2211.
35. Chedin,F. and Kowalczykowski,S.C. (2002) A novel family of regulated helicases/nucleases from Gram-positive bacteria: insights into the initiation of DNA recombination. *Mol. Microbiol.*, **43**, 823–834.
36. Chedin,F., Seitz,E.M. and Kowalczykowski,S.C. (1998) Novel homologs of replication protein A in archaea: implications for the evolution of ssDNA-binding proteins. *Trends Biochem. Sci.*, **23**, 273–277.
37. Chedin,F., Ehrlich,S.D. and Kowalczykowski,S.C. (2000) The Bacillus subtilis AddAB helicase/nuclease is regulated by its cognate Chi sequence in vitro. *J. Mol. Biol.*, **298**, 7–20.
38. Byrd,A.K. and Raney,K.D. (2004) Protein displacement by an assembly of helicase molecules aligned along single-stranded DNA. *Nat. Struct. Mol. Biol.*, **11**, 531–538.
39. Morris,P.D. and Raney,K.D. (1999) DNA helicases displace streptavidin from biotin-labeled oligonucleotides. *Biochemistry*, **38**, 5164–5171.
40. Iordanescu,S. and Bargonetti,J. (1989) Staphylococcus aureus chromosomal mutations that decrease efficiency of Rep utilization in replication of pT181 and related plasmids. *J. Bacteriol.*, **171**, 4501–4503.
41. Petit,M.A., Dervyn,E., Rose,M., Entian,K.D., McGovern,S., Ehrlich,S.D. and Bruand,C. (1998) PcrA is an essential DNA helicase of Bacillus subtilis fulfilling functions both in repair and rolling-circle replication. *Mol. Microbiol*, **29**, 261–273.
42. Noirot,P., Bargonetti,J. and Novick,R.P. (1990) Initiation of rolling-circle replication in pT181 plasmid: initiator protein enhances cruciform extrusion at the origin. *Proc. Natl Acad. Sci. USA*, **87**, 8560–8564.
43. Roman,L.J. and Kowalczykowski,S.C. (1989) Characterization of the helicase activity of the Escherichia-coli RecBCD enzyme using a novel helicase assay. *Biochemistry*, **28**, 2863–2873.
44. Serebrov,V. and Pyle,A.M. (2004) Periodic cycles of RNA unwinding and pausing by hepatitis C virus NS3 helicase. *Nature*, **430**, 476–480.
45. Roy,R., Kozlov,A.G., Lohman,T.M. and Ha,T. (2009) SSB protein diffusion on single-stranded DNA stimulates RecA filament formation. *Nature*, **461**, 1092–1097.